

A RECONFIGURABLE L-BAND ACTIVE ARRAY FOR SATELLITE COMMUNICATIONS

K.S. Rao, H. Gauvin, G. Goyette and S. Richard
Satellite & Communications Systems Division
Spar Aerospace Limited, Ste-Anne-de-Bellevue
Quebec, Canada H9X 3R2

ABSTRACT

Design and experimental results of an L-band active array for mobile satellite communication antennas are presented in this paper. A receive feed array consisting of seven active modules is breadboarded. Each module consists of a circularly polarized radiating element, a stripline filter, a low-noise amplifier, a variable attenuator and a variable phase shifter. The output ports of the active modules are combined using a 7 to 1 beamforming network. Measured results of the septet array demonstrate that the beam shape can be reconfigured from 16° to 48° half-power beamwidth while the beam location can be reconfigured over $\pm 16^\circ$ angular region. Low sidelobe and cross-polar levels have been maintained for the active array over the scan region.

INTRODUCTION

The antenna systems for future satellites are expected to be designed with more in-orbit reconfiguration features. These can range from scanning of the beams to reconfiguring the beam shape by employing active technology for the antennas. For example, future generation Inmarsat satellites are likely to carry multi-mission mobile payloads to support different types of services such as global and regional coverages at L-band. The global mission continues to provide international communication to Maritime and aeronautical mobile earth stations with increased capacity while the regional mission provides communication to new smaller mobile earth stations on a regional basis. The high gain regional spot beams are reconfigurable over the global field of view. These objectives are broadly driving the present design of an L-band multibeam receive antenna.

This paper addresses the breadboard development of a small active array that could meet various reconfigurability requirements. The design of the receive antenna is presented along with experimental results of the following components (a) circularly polarized radiating element, (b) stripline filter, (c) active components and (d) beamforming network. Results of the beam reconfigurability measurements of the active array are also discussed.

This work was jointly supported by the Department of Communications, Ottawa, and Spar under contract No. SDP-86-007.

ANTENNA DESCRIPTION

The antenna system considered for a mobile payload consists of an offset parabolic reflector fed with a focal-plane active array. A deployable mesh reflector with significant dimensions as shown in Figure 1 is chosen. The feed array consists of 61 radiating elements arranged in hexagonal grid for efficient overlap of regional beams. The global, global spot and regional beams are generated using 61, 20 and 7 elements of the feed array respectively. Spacing between the radiating elements is a trade-off between the antenna performance and the feed array complexity. A $1.1 \lambda_0$ inter-element spacing is selected for the array. The grating lobes appearing in the visible space are not intercepted by the reflector and hence do not affect the secondary patterns significantly. The gain contours are optimized by the SCOPE software developed by TICRA and minimum EOC directivity values of 20, 25 and 32.4 dBic are achieved for the global, global spot and regional beams. Synthesized gain contours for global spot beams are shown in Figure 2. For the present development, a feed array consisting of seven elements to generate one regional beam is considered. The active feed array configuration is shown in Figure 3. Beam reconfigurability is achieved using the variable attenuators and variable phase shifters.

DEVELOPMENT OF ARRAY COMPONENTS

a) Radiating Element: The radiating element is circularly polarized and covers a bandwidth of 1.8% with centre frequency as 1.64 GHz. Helical radiator is selected for the breadboard array because of its superior cross-polar characteristics. The helix radiator is backed by a circular cavity in order to minimize the back radiation and also to reduce the mutual coupling among the array elements. Helical windings are made using copper plated steel springs and are supported by a 0.25" thick high-impact polystyrene. It has 8 turns with the last three being tapered to improve the axial ratio. The circumference of the axial mode helix is $1.168 \lambda_0$ and the pitch angle is 12.5° . The circular cup has a diameter of $0.84 \lambda_0$ and a length of $0.5 \lambda_0$. A matching transformer is used near the feed-end of the helix to convert the 50Ω coaxial impedance to the 150Ω input impedance of the helix. Measured return loss is better than 30dB over the receive band. Figure 4 shows the radiation patterns of the helix measured using a rotating linearly polarized source. Axial ratio of the helix is measured less than 0.25dB on-axis and less than 0.75dB within the illuminated region ($\pm 28^\circ$) of the reflector over the desired band. Breadboard model of the feed array is shown in Figure 5.

b) Receive Filter and Active Module: A filter is connected between each radiating element and the active module in order to isolate the receiver from the transmit signal. The filter is designed to provide 80dB isolation for transmit signals (1.53 to 1.56 GHz). A

Tchebysheff filter with 9 resonators is breadboarded using the stripline medium with electroplated copper on RF Duroid 5880 ($\epsilon_r = 2.2$). A large ground plane spacing (0.25") is used to increase the line widths and to minimize the conduction losses. The filter response is shown in Figure 6. Return loss of the filter is better than 16dB over the receive band. The block diagram of the active module is shown in Figure 7. All components of the module have been realized using the MIC technology. An isolator is used before the LNA in order to provide a good match. The LNA circuitry is adjusted for minimum noise figure. Two variable phase shifters and a variable attenuator are used to provide up to 200° phase shift and a maximum attenuation of 40dB. The overall gain of the active module (with no attenuation) is measured as 32dB and the noise figure is 1.4dB. The bandpass filter is integrated with active module using a ribbon connection and the breadboard assembly is shown in Figure 8.

c) Beamforming Network: A 7 to 1 low-level BFN is used to combine the signals from the outputs of the seven active modules. The insertion loss of the BFN is not critical since it is placed after LNA. The BFN is designed with outer elements being excited at -11dB amplitude relative to the central element. The BFN is implemented using a microstrip medium consisting of a cascade of branch-line couplers, matched loads, transformers and bends. It is etched on a 0.025" thick Duroid with $\epsilon_r=10.5$ as shown in Figure 9. Measured return loss of the BFN is better than 16dB.

BEAM RECONFIGURABILITY MEASUREMENTS OF ACTIVE ARRAY

A tile array architecture shown in Figure 10 has been selected for the active array integration. This architecture has a minimum number of physical connections between different layers of the array. The outputs of the helices are connected to the filter input using a short length of the semi-rigid cable and a surface mount connector. Breadboard model of the integrated array is shown in Figure 11. Measured excitations of the active array (excluding the radiating elements) are shown in Table 1. The radiation pattern of the active array with nominal excitations is shown in Figure 12. It has been measured with a rotating linearly polarized source antenna. The antenna has low axial ratio (less than 1.0 dB over the band) and the sidelobe levels are better than 26 dB over the receive band.

Figure 13 shows measured patterns of the active array demonstrating the beam shape reconfigurability. They have been measured by varying the bias of the attenuators while keeping zero bias for the phase shifters. The patterns shown in Figure 13 indicate that the half-power beamwidth of the antenna can be reconfigured from 16° to 48°. Beam location reconfigurability measurements are given in Figure 14. Different beams are generated by varying the bias of the phase shifters with zero bias on all attenuators. The phase shifter bias values are pre-determined based on the required phase shift values for the array elements. All the beams shown in Figure 14 have low sidelobe levels over the scan region. The antenna beam

of the active array can be reconfigured over ± 16 degrees along the elevation and the azimuth directions.

CONCLUSIONS

The breadboard results presented in this paper demonstrate the potential application of active arrays for future satellite communication antennas where in-orbit reconfigurability of antenna patterns is required over the global field-of-view. The active technology has also the advantage over passive technology that the beam forming can be realized at low-level using light weight and cost-effective BFNs.

TABLE 1 ACTIVE ARRAY MEASURED EXCITATIONS*
(BFN + ACTIVE MODULES + CABLES)

ELEMENT #	F = 1.631 GHz		F = 1.646 GHz		F = 1.661 GHz	
	AMPL. (DB)	PHASE (DEG)	AMPL. (DB)	PHASE (DEG)	AMPL. (DB)	PHASE (DEG)
1	30.03	0	29.58	0	28.87	0
2	19.42	18.8	19.25	12.4	19.25	8.6
3	18.58	-5.0	18.62	-5.2	18.80	-2.2
4	16.62	24.3	17.34	15.0	19.12	11.1
5	20.77	23.4	19.54	2.3	19.03	14.6
6	18.63	-21.1	16.92	-10.0	16.34	9.4
7	17.34	-6.5	15.85	-11.9	12.39	0.6

* All the attenuators and phase shifters are set to zero volts bias.

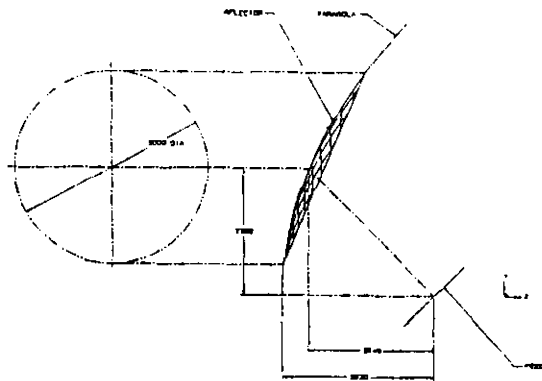


FIGURE 1: L-BAND REFLECTOR ANTENNA GEOMETRY

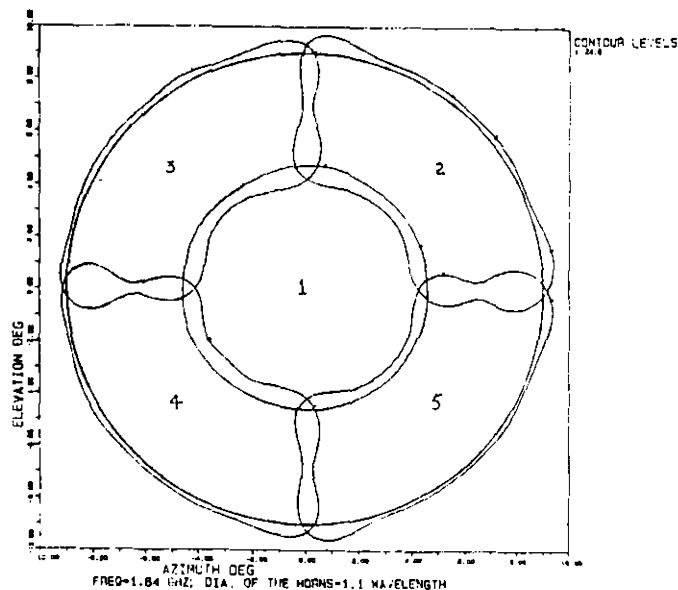


FIGURE 2: OPTIMIZED GAIN CONTOUR PLOT FOR THE GLOBAL SPOT BEAMS

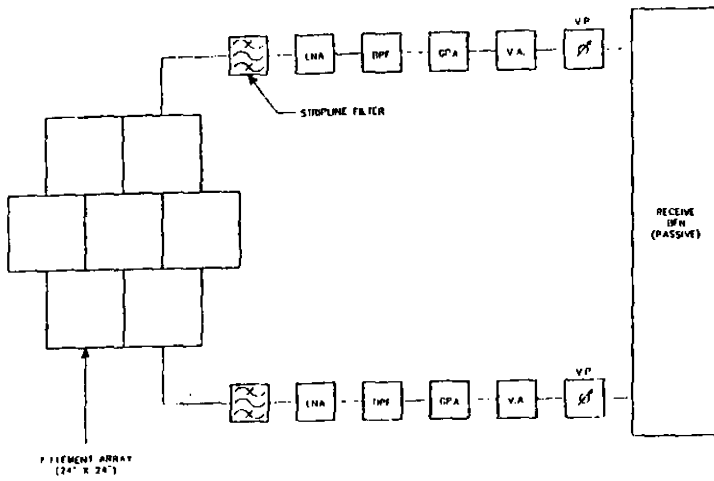


FIGURE 3: FEED ARRAY CONFIGURATION FOR THE BREADBOARD ACTIVE ARRAY

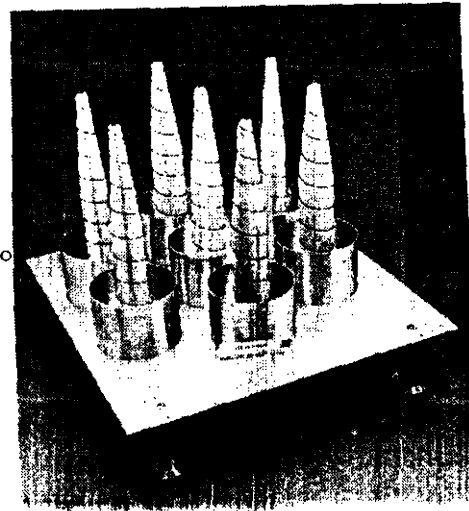


FIGURE 5: BREADBOARD MODEL OF THE HELICAL ARRAY

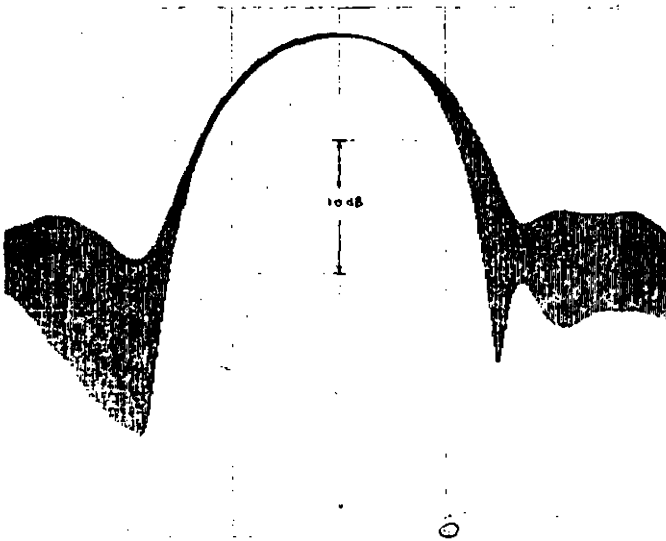


FIGURE 4: MEASURED CP RADIATION PATTERNS OF THE HELIX RADIATOR ($F = 1.646$ GHz)

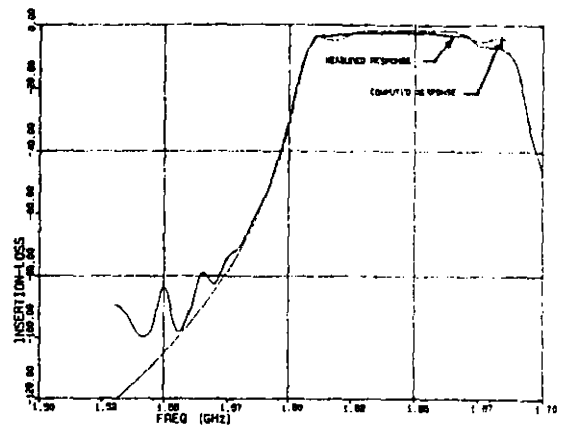


FIGURE 6: MEASURED INSERTION LOSS RESPONSE OF THE RECEIVE FILTER

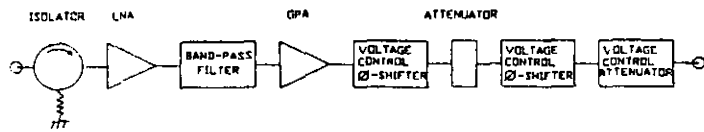


FIGURE 7: BLOCK DIAGRAM OF THE ACTIVE MODULE

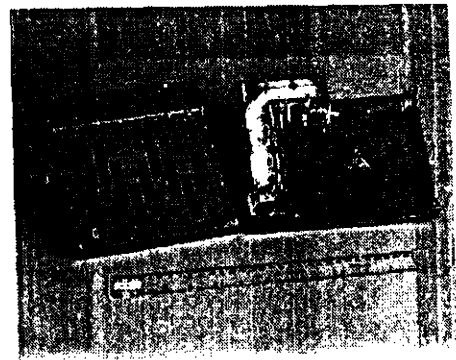


FIGURE 8: BREADBOARD MODEL OF THE ACTIVE MODULE SHOWING THE TOP AND BOTTOM SIDES

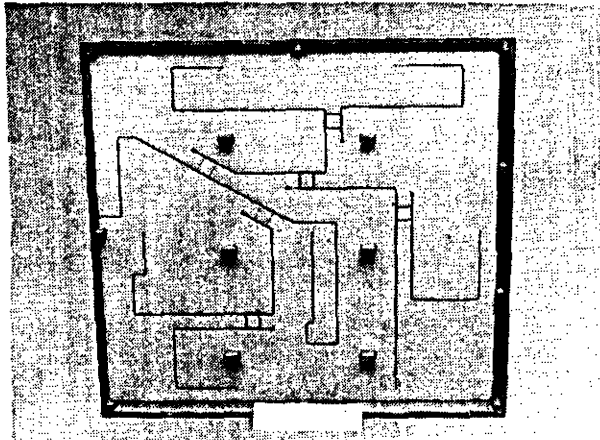


FIGURE 9: BREADBOARD MODEL OF THE 7 TO 1 PASSIVE BEAMFORMING NETWORK

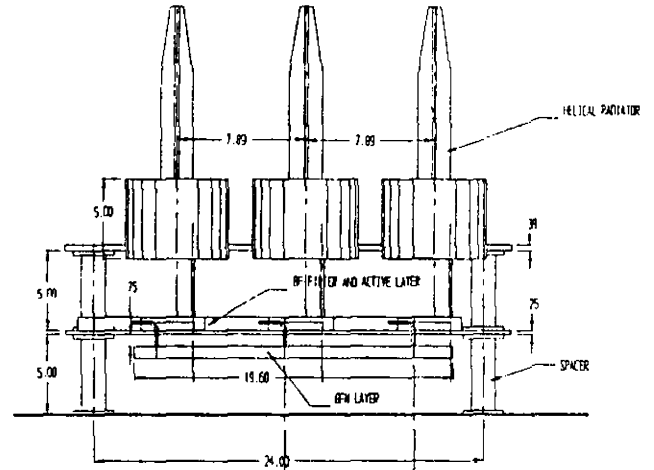


FIGURE 10: ARCHITECTURE FOR THE L-BAND ACTIVE ARRAY



FIGURE 11: BREADBOARD MODEL OF THE INTEGRATED ARRAY

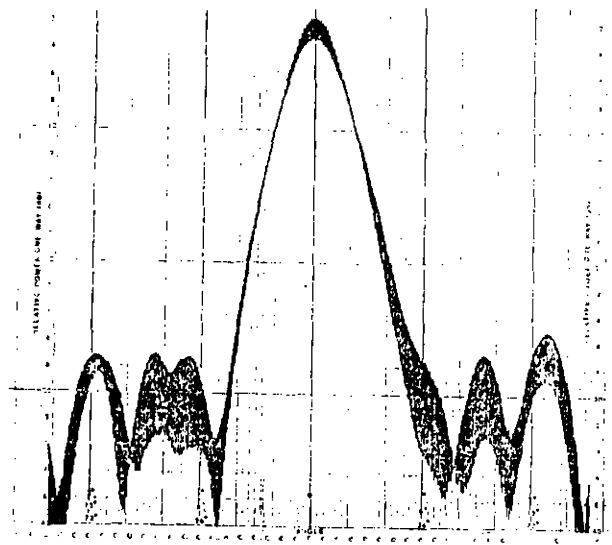


FIGURE 12: MEASURED RADIATION PATTERNS OF THE ACTIVE ARRAY WITH NOMINAL EXCITATIONS ($F = 1.646$ GHz)

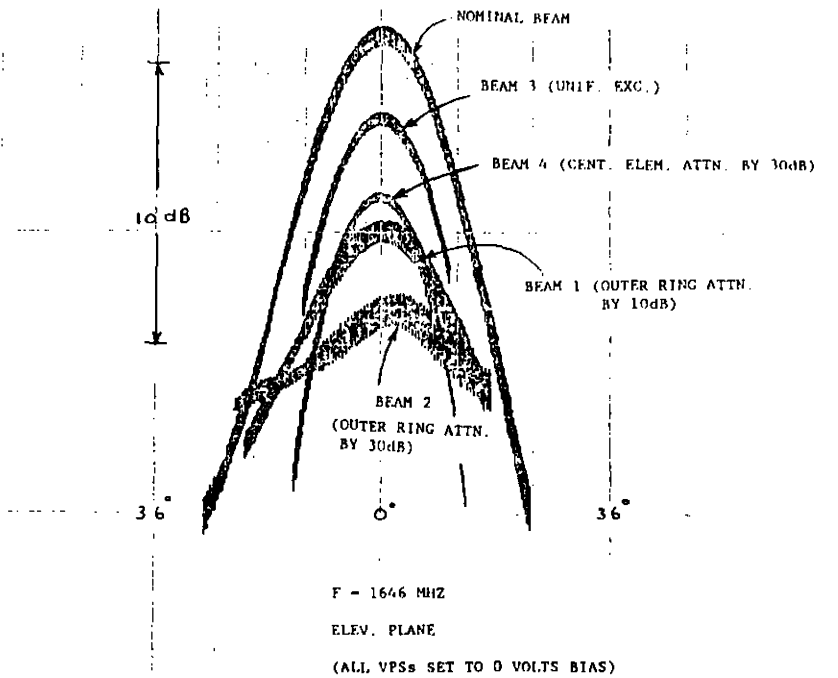


FIGURE 13: BEAM SHAPE RECONFIGURABILITY MEASUREMENTS OF THE ACTIVE ARRAY

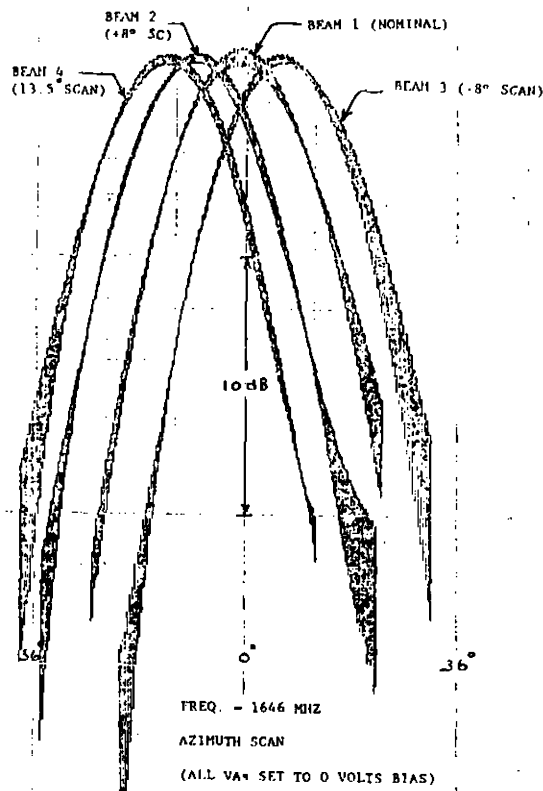


FIGURE 14: BEAM LOCATION RECONFIGURABILITY MEASUREMENTS OF THE ACTIVE ARRAY